ACI STRUCTURAL JOURNAL TECHNICAL PAPER

Title no. 108-S17

Shear Deformations of Slender Reinforced Concrete Walls under Seismic Loading

by Katrin Beyer, Alessandro Dazio, and M. J. Nigel Priestley

Experimental results gained from quasi-static cyclic tests on 34 slender structural reinforced concrete walls available in the literature are used to examine the shear deformations for displacement demands in the inelastic range. Based on these results, the distribution of shear strains within the walls and the variation of shear deformations with top displacements is discussed. It is shown that for shear walls whose shear-transfer mechanism is not significantly deteriorating, the ratio of shear-to-flexural deformations remains approximately constant over the entire range of imposed displacement ductilities, whereas for walls whose shear-transfer mechanism is significantly degrading, the ratio of shear-to-flexural deformations increases. For the former, a simple model is proposed that allows the estimation of the ratio of shear-to-flexural deformations.

Keywords: cyclic tests; instrumentation; reinforced concrete; shear deformations; structural walls.

INTRODUCTION

Slender reinforced concrete (RC) walls, which are designed to have a larger shear resistance than flexural resistance, and whose behavior is therefore controlled by flexure rather than shear, behave in a ductile flexural mode when loaded beyond the elastic limit. The inelastic seismic behavior of such walls can be analyzed using advanced models that account for the biaxial in-plane stress state in the RC elements, such as the modified compression field theory by Vecchio and Collins,[1] on which the Response-2000[2] and VecTor2[3] programs are based. Other advanced modeling approaches that have been developed to analyze the inelastic response of RC members are based on macroelements, such as the PERFORM[4] program, in which different layers of the macroelements are assigned a specific load-carrying mechanism, such as axial forces and bending moments or shear forces. In engineering practice, however, slender walls are still often modeled with beam elements. The formulation of the most common types of nonlinear beam elements (that is, displacement-based[5] or force-based inelastic beam elements[6]) focuses on modeling the flexural rather than the shear response of the member. As a result, relative elaborate techniques are available for modeling the inelastic flexural response, such as models with inelastic beam elements with fiber sections. Compared to the options that are available to engineers when modeling the flexural response of RC members, the variety of approaches for modeling the shear response is relatively sparse. In most structural engineering programs, the shear stiffness of beam elements that develop a flexural mechanism is assigned a constant value that cannot be updated during the loading process. This modeling approach has been supported by the misconception that—because the shear reinforcement is not supposed to yield and the compression strut is not supposed to crush—the shear deformations will remain constant once the nominal yield force has been reached. Although experimental evidence that proved this conclusion wrong has been available for many decades, it has not often been considered when modeling slender RC walls. Hence, regarding the acknowledgement of the magnitude of the shear deformations, a vicious circle was created, wherein shear deformations in structural analyses are underestimated due to excessively large shear stiffness values. Their contribution to the total deformations are therefore perceived as negligible and their effect on the structural performance is not considered.

The objective of this paper is to present experimental data for the shear deformations of slender cantilever walls by examining the data of 34 test units available in the literature with an aspect ratio larger than 2 that were subjected to quasi-static cyclic loading and to identify parameters that affect the shear deformations. Of particular interest is the ratio of shear-to-flexural deformations when the wall is loaded in the inelastic range to conclude whether shear deformations are important to consider in structural analysis. Based on these results, shear displacements can be estimated or the effective stiffnesses of beam elements can be determined.

RESEARCH SIGNIFICANCE

The purpose of this paper is: 1) to examine the shear deformations in rectangular and nonrectangular RC walls; and 2) to provide estimates of the expected shear deformations in walls controlled by flexure that can be used for computing shear deformations for plastic-hinge analysis or for deriving equivalent elastic shear stiffnesses representative of a certain displacement ductility level for use in other types of analyses, such as the analysis of models with inelastic beam elements.

DETERMINING SHEAR AND FLEXURAL DEFORMATIONS FROM EXPERIMENTAL MEASUREMENTS

The total top displacement of a cantilever RC wall can be interpreted as the sum of three displacement components—that is, 1) the flexural displacement Δ_f, which is the sum of the flexural deformations Δ_f' of the wall panel and the displacement Δ_θ caused by the fixed-end rotation of the wall associated with the strain penetration of the longitudinal reinforcing bars into the foundation; 2) the shear deformations Δ_s of the wall; and 3) the sliding displacement Δ_{sl} along the joint between the wall and foundation. For typical wall designs, the sliding displacements are relatively small and

ACI Structural Journal, V. 108, No. 2, March-April 2011.
MS No. S-2008-281.R3 received January 19, 2010, and reviewed under Institute publication policies. Pertinent discussion including author's closure, if any, will be published in the January-February 2012 *ACI Structural Journal* if the discussion is received by September 1, 2011.

ACI member **Katrin Beyer** *is an Assistant Professor of Earthquake Engineering at the Ecole Polytechnqiue Fédérale de Lausanne (EPFL) in Lausanne, Switzerland. She received her PhD from the Rose School, Pavia, Italy. Her research interests include large-scale structural tests, the seismic behavior of nonrectangular reinforced concrete (RC) walls and unreinforced masonry structures, and the torsional response of asymmetric buildings when subjected to seismic excitation.*

ACI member **Alessandro Dazio** *is Deputy-Director of the Rose School and Coordinator of the Reinforced Concrete research section of the EUCENTRE Foundation in Pavia, Italy. His research interests include the seismic design and assessment of RC and masonry structures through large-scale structural testing, numerical simulation, and analytical models.*

M. J. Nigel Priestley, *FACI, is a Professor Emeritus at the University of California at San Diego, San Diego, CA, and Co-Director Emeritus of the Rose School. He received the ACI Raymond C. Reese Structural Research Award in 1984 and 1989, the ACI Wason Award for Most Meritorious Paper in 1997, and the ACI Arthur R. Anderson Award in 1997. His research interests include the seismic design, assessment, and retrofit of RC bridges and buildings; seismic design philosophy for precast concrete structures; and development of realistic dynamic testing methods to simulate inelastic response under seismic loading.*

are therefore not discussed any further. The following two sections outline the instrumentation layouts and evaluation techniques for determining the shear and flexural displacement components from the wall tests.

Typical instrumentation layouts for determining displacement components

Possible layouts for determining the different displacement components are discussed, using the instrumentation of the U-shaped walls that were tested by the authors under quasi-static cyclic loading[7] as an example. The main objective of these tests was to compare the behavior of the U-shaped walls for different directions of loading. Because the results of these tests are also used in the following sections, a brief description of the test setup and the loading history is given herein; for further details, refer to Beyer et al.[7] The cross sections, aspect ratios, and axial load ratios of the two test units TUA and TUB are given in Table 1. By means of three actuators (Fig. 1(a)), the walls were subjected to a complex bidirectional loading history (Fig. 1(b)) in which five different directions of loading were distinguished and labeled with different letters: 1) parallel to the web (Positions A and B); 2) parallel to the flanges so that the flange ends are in compression (Position C); 3) parallel to the flanges so that the web is in compression (Position D); 4) in a diagonal direction so that one flange end is in compression (Positions E and H); and 5) in a diagonal direction so that one corner is in compression (Positions F and G). At each ductility level, the wall was first subjected to a cycle parallel to the web, a cycle parallel to the flanges, a cycle in a diagonal direction, and a "sweep."

The instrumentation of the U-shaped walls was such that the displacement components of the web and the two flanges could be separately determined. Figure 2 shows the continuous chains of linear variable differential transformers (LVDT) measurements, which were taken along the four outer edges of the U-shaped wall. Such LVDT chains are used in most wall tests for determining average curvatures along the wall height; for walls tested under unidirectional loading, two chains instead of four are sufficient. When designing the instrumentation for a test unit, the researcher typically strives for as many detailed measurements as possible, while at the same time limiting the number of instruments needed. For this reason, it is common to choose LVDTs with smaller base lengths for regions where inelastic deformations are expected to cause large curvature gradients and LVDTs with larger base lengths for regions that remain largely elastic where the curvature gradient is smaller. For good estimates of the flexural top displacement, it is typically advisable to determine the displacement due to the fixed-end rotation Δ_θ independently of the displacement due to the flexural deformation of the wall Δ_f'. The base length of the lowest member of the LVDT chain should therefore be so short that the instrument only extends over the base crack between the wall and foundation and does not cross any other large cracks.

For determining the shear deformations, diagonal measurements are taken (Fig. 2(a)). To cover approximately the height of one inclined flexure-shear crack, values in the order of the wall length are often chosen for the height of the shear panel, but smaller heights have also been used in the past.[8,9] When the lowest points of the diagonal measurements are fixed to the wall rather than the foundation, the measured shear deformation does not include any sliding movement Δ_{sl} along the construction joint between the foundation and the wall; in this case, the sliding movement has to be separately measured using additional LVDTs[7] (Fig. 2).

Computation of displacement components from experimental measurements

Due to the presence of "cracking, plane sections not remaining plane, and the existence of a moment gradient across the element,"[8] as well as the fact that the subdivision of deformations of inelastic RC wall members into shear and flexural deformations is—to some extent—artificial, the displacement components determined from experimental measurements are only approximate values. Although they are not exact, however, they provide a useful link between the experiments and numerical models, particularly if beam models are used. Average curvatures can be derived from the chains of LVDTs along the edges of the walls, and the flexural deformations Δ_f' can be computed by integrating the curvatures twice. The total flexural displacement Δ_f' is computed as the sum of Δ_f' plus the wall displacement due to the fixed-end rotation Δ_θ, which is associated with strain penetration into the foundation. Unlike for the experimental flexural deformations, which are mostly determined by the method described previously, and where differences between test series on RC walls chiefly originate from different base lengths of the LVDT measurements rather than the evaluation method, the evaluation of shear deformation is less homogenous between different research groups. For many test series, the shear displacements of a shear panel have been evaluated using one of the following two equations

$$\Delta_s = \frac{1}{4b}((d+\delta_2)^2 - (d+\delta_1)^2) \tag{1a}$$

$$\Delta_s = \frac{d}{2b}(\delta_2 - \delta_1) \tag{1b}$$

where b is the width of the shear panel, d is the original length of the diagonal, and δ_i is the change in length of one of the two diagonals. Equation (1(b)) corresponds to the zero and first order terms of the Taylor series of Eq. (1(a)). Hiraishi[10] showed that these approaches are only correct if the curvature is constant over the height of the panel for which the shear displacements are determined and, therefore, any difference in the lengths of the diagonals is associated

Table 1—Cross sections of isolated cantilever walls tested under quasi-static cyclic loading that were included in this study (all dimensions in mm; 1 mm = 0.0394 in.)

Test Unit	Cross section	H_n/l_w ν[1)]	Test Unit	Cross section	H_n/l_w ν	Test Unit	Cross section	H_n/l_w ν
Dazio *et al.*[11]						**Hines *et al.*[12,13]**		
WSH1	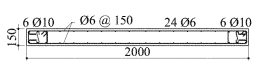	2.3 5.1%	WSH4	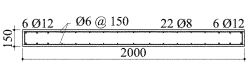	2.3 5.7%	1A	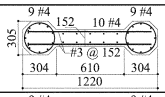	4.0 10.0%
WSH2	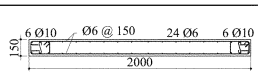	2.3 5.7%	WSH5	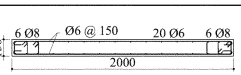	2.3 12.8%	1B	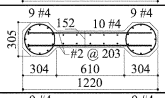	4.0 10.0%
WSH3	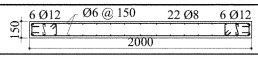	2.3 5.8%	WSH6	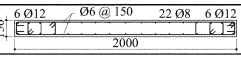	2.3 10.8%	2A	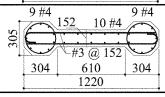	2.0 10.0%
PCA, Phase I[8]			**PCA, Phase II[9]**					
R1	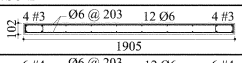	2.4 0.4%	B6	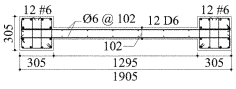	2.4 13.4%	2B	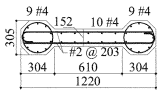	2.0 10%
R2	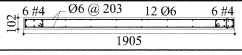	2.4 0.4%						
B1	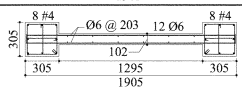	2.4 0.3%	B7	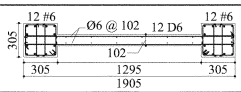	2.4 7.6%	2C	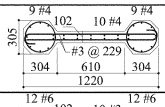	2.0 10.0%
B3	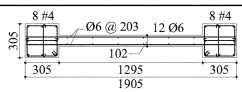	2.4 0.3%	B8	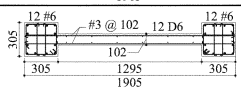	2.4 9.0%	3A	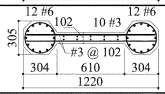	2.5 9.3%
B2	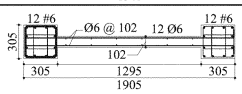	2.4 0.3%	B9	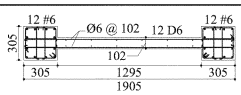	2.4 8.5%	3B	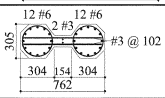	2.5 7.5%
B5	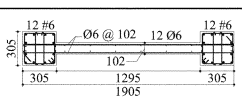	2.4 0.3%	B10	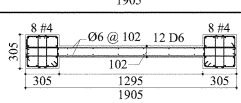	2.4 8.2%	3C	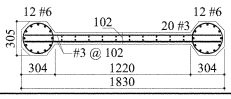	2.5 8.7%
F1	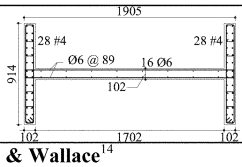	2.4 0.4%	F2	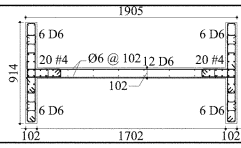	2.4 7.3%			
Thomson & Wallace[14]								
RW1	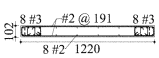	3.1 10%	TW1	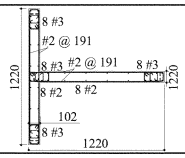	3.1 9%	TW2	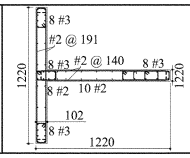	3.1 7.5%
RW2	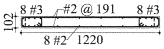	3.1 7%						
Pégon *et al.*[15-18]			**Beyer *et al.*[7]**					
	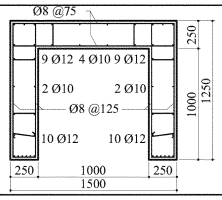	3.2/ 2.6[2)] 10.2%-11.6%[3)]	TUA	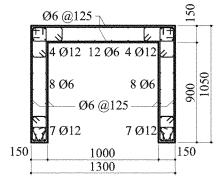	2.8/ 2.6[2)] 2.2%	TUB	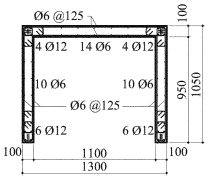	2.8/ 2.6[2)] 4.5%

1) $\nu=N/(A_{gross}f_c')$
2) Depending on the direction of loading.
3) Three specimens with the same reinforcement layout were built and subjected to the same axial load. The concrete strength varied slightly between the three units.

with shear deformations only. If the curvature is not constant over the height of the shear panel—as is the case for cantilever walls—part of the difference in the lengths of the diagonals has to be attributed to flexural deformations. This is illustrated in Fig. 3. Consequently, Eq. (1(a)) and (1(b)) overestimate the actual shear deformation if the curvature is not constant over the height of the shear panel. Hiraishi[10] also showed that a term needs to be subtracted to account for the variation of curvature over the height of the panel

$$\Delta_s = \frac{1}{4b}((d+\delta_2)^2-(d+\delta_1)^2)-(\alpha-0.5)\theta(h_{sh})h_{sh} \quad (2)$$

where $\theta(h_{sh})$ is the difference of rotations at the top and bottom of the panel of height h_{sh} for which the shear deformations are determined, and α is a measure for the variation of the curvature over the height of the panel. The values of α vary between 0.5 and 1 if the point of contraflexure is above the panel for which the shear deformations are determined

$$\alpha = \frac{\int_0^{h_{sh}} \theta(z)dz}{\theta(h_{sh})h_{sh}} \quad (3)$$

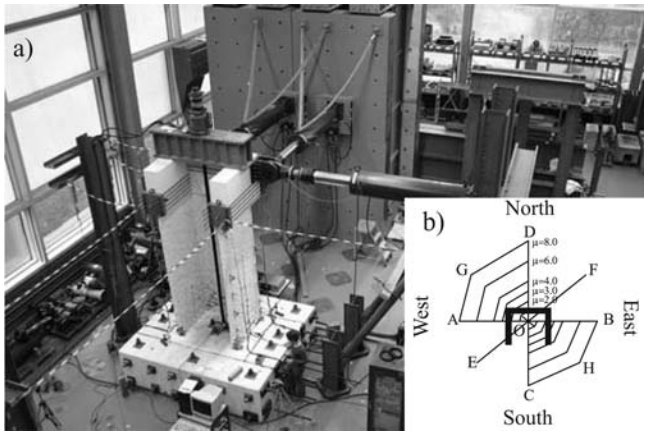

Fig. 1—Quasi-static cyclic tests on U-shaped walls[7]: (a) test setup; and (b) loading history with cardinal points.

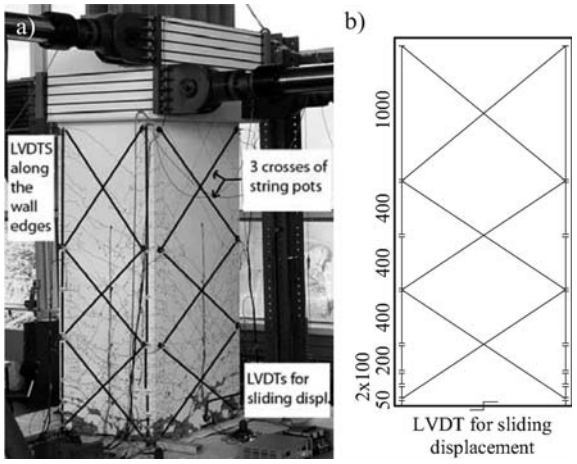

Fig. 2—Instrumentation of U-shaped walls[7]: (a) instrumentation suitable for determining different displacement components Δ_f, Δ_θ, and Δ_s (photo); and (b) sketch of instrumentation of one flange. (Note: all dimensions are in mm; 1 in. = 25.4 mm.)

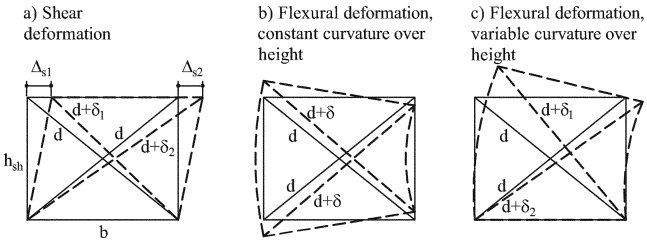

Fig. 3—Variation of length of shear panel diagonals: (a) for shear; (b) for flexural deformations with constant curvature over height; and (c) with variable curvature over height.

For a constant curvature, α is 0.5 and Eq. (2) yields the original Eq. (1(a)) and (1(b)). If the curvature distribution is triangular, α equates to 2/3; and if the deformations are concentrated near the base, α tends toward unity. Provided that the base lengths of the LVDTs measuring the elongations of the wall edges are shorter than the height of the shear panel, the value of α can be computed from these LVDT measurements. Massone and Wallace[19] studied a hypothetical case and judged that four to six LVDTs with equal base lengths over the height of one shear panel would be sufficient to yield good estimates of α. The authors use LVDT base

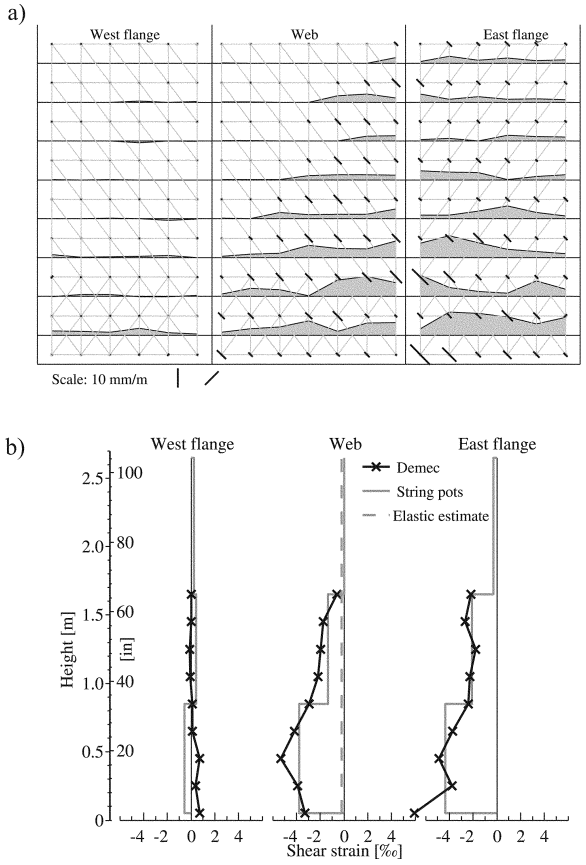

Fig. 4—Distribution of shear and axial strains for U-shaped wall TUA[7] at μ_Δ = 3.0 for Position A: (a) shear strains obtained from Demec measurements (thin lines illustrate Demec measurement grid, whereas thick lines represent shear strains and grey shaded areas represent axial strains); and (b) comparison of shear strains obtained from Demec measurements to shear panel measurements (dashed line represents shear strain corresponding to shear stiffness G_cA_w).

lengths that vary over the wall height (Fig. 2). The base lengths are chosen to yield good estimates of the flexural deformations Δ_f, which yields generally sufficient accurate values of α because α is a direct measure of Δ_f. For slender walls, the wall is typically divided into several shear panels over its height (Fig. 2). The shear deformations of each panel are computed from a pair of diagonal measurements. The shear deformation of the wall over its entire height is the sum of the shear deformations of all panels.

EXPERIMENTAL EVIDENCE OF SHEAR DEFORMATIONS

Distribution of shear strains within RC wall

Although the shear force in a cantilever wall subjected to a point load at the top is constant over the height, the shear strains are far from being evenly distributed over the height and section once the wall has cracked and the longitudinal reinforcement yields. This is illustrated by the results obtained from the Demec measurements (Whitmore gauge measurements) taken during the U-shaped wall tests, which allow the visualization of the strain distribution over the wall face. At each Demec measurement point, the strain state is determined from its relative movement to its surrounding measurement points. Demec measurements were taken on the inside faces of the wall, whereas the outer faces were

used for LVDT chains and shear-panel measurements, as described in the previous section. For example, the shear and axial strain distribution of the U-shaped wall TUA at a displacement ductility $\mu_\Delta = 3.0$ when the wall is orthogonally loaded to its symmetry axis (Position A) is plotted in Fig. 4(a). The figure shows that the shear strains are concentrated in the plastic zone, particularly in areas where large tensile longitudinal steel strains were encountered. Hence, the results suggest that the magnitude of the shear strains is directly linked to the magnitude of the tensile strains in the vertical reinforcing bars. The link has also been observed, for example, by Vallenas et al.,[20] Oesterle et al.,[21] and Thomson and Wallace.[14] Figure 4(b) shows a comparison of the shear strains obtained from Demec measurements to the shear strains obtained from the shear-panel instrumentation. For the comparison, the Demec measurements of each wall section (that is, the two flanges and the web) were averaged at the heights of the Demec measurement points. The resolution of the Demec measurements is, of course, significantly higher over the height than the distribution of the shear strains obtained by the shear-panel measurements; however, the figure shows a good agreement between the two methods of determining the shear deformations. Also included in Fig. 4 is a vertical dashed line, which corresponds to the shear strains obtained for a shear stiffness value of $0.4E_cA_w$, which is recommended by FEMA 356[22] for the elastic analysis of RC walls. In this equation, A_w is the wall area between the extreme compression fiber and the center of the tension reinforcement, which shall be typically assumed as $0.8b_wl_w$,[23] where b_w and l_w are the width and length of the wall, respectively. Assuming that the shear modulus G_c of concrete can be estimated as 40% of the elastic modulus E_c, the suggested shear stiffness corresponds to G_cA_w, which is for $A_w = 0.8A_g$ only approximately 7% smaller than the shear stiffness of an elastic homogenous uncracked member. The effective shear area of an elastic homogenous uncracked member with a slender section is $A_w = (5 + 5\nu)/(6 + 5\nu)A_g$[24] and equates to $A_w = 0.86A_g$ for $\nu = 0.2$, which is a typical Poisson's ratio of concrete. The comparison with the shear deformations derived from measurements underlines that computing the shear deformation based on elastic properties significantly underestimates the shear deformations of members with shear cracking.[19]

Shear force-shear displacement hysteresis

In many analyses of RC structural walls controlled by flexure, it is assumed that the shear stiffness of the wall remains approximately constant after the shear crack pattern has fully developed and the wall is loaded in the inelastic range. Because the shear force carried by a wall only marginally increases once the nominal yield force has been reached, this modeling approach predicts that for displacements beyond the yield displacement, the shear displacement remains approximately constant, whereas the flexural displacement increases. Experimental results show that this is not the case. Although the behavior of the wall is dominated by flexure, the shear displacement-shear force hysteresis in Fig. 5 is highly nonlinear and the shear deformations increase with increasing top displacement. The hysteresis also shows that the shear displacement varies the most when the lateral load is close to 0: at this point, the cracks are open along their entire length and therefore the resistance against relative movements of the crack interfaces is small. As a result, the shear stiffness is very low and leads to the "pinching" of the

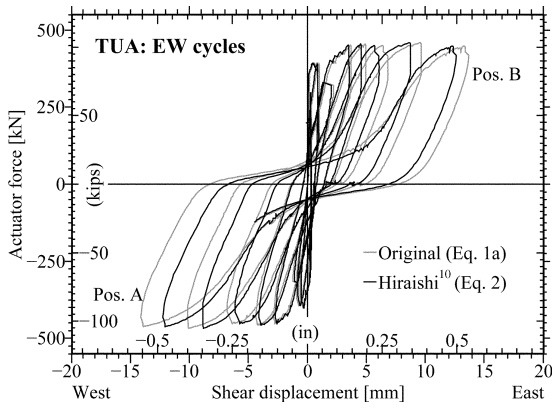

Fig. 5—Shear displacement-shear force hysteresis for U-shaped wall TUA[7] for cycles parallel to web and restrained wall head rotation. Plot includes shear displacements according to Eq. (1a) and (2).

force-deformation hysteresis.[25] To give an idea of the difference between the two methods of evaluating the shear displacements that were discussed in the previous section, results for both methods—Eq. (1(a)) and (2))—are included in Fig. 5. For the results presented herein, the difference in peak shear displacements is between 5 and 12%. Massone and Wallace,[19] however, reported differences as large as 31% for the two methods of evaluating the shear deformations. The obtained difference depends on the curvature profile over the height of the shear panel, the magnitude of the α factor, and the ratio of shear-to-flexural deformations of the shear panel.

Variation of Δ_s/Δ_f ratio with ductility demand

The shear strain distribution (Fig. 4) and the hysteresis curve (Fig. 5) suggest that the magnitude of the shear deformations does not only depend on the shear force but also depends on the inelastic flexural deformations. Experimental evidence for the continuous growth of the shear deformations with top displacements when the wall is loaded in the inelastic range was presented in the 1970s by Wang et al.,[26] Vallenas et al.,[20] and Oesterle et al.[8,9] Vallenas et al.,[20] for example, observed that yielding of the shear and flexural mechanism simultaneously occurs, and that even if the shear stresses were constant over the height of the wall, shear yielding is only observed in regions where the flexural mechanism yields. Vallenas et al.[20] also stated that for the monotonic loading, the shear deformations "were almost a constant factor of the flexural deformations," whereas for specimens subjected to cyclic loading, the ratio of shear-to-flexural deformations "increases with the number of load reversals and intensity of the deformation." Vallenas et al.'s[20] findings are revisited in the following section using the results from different series of quasi-static cyclic wall tests as evidence.

The considered test series are the following: 1) Phases I and II of the PCA tests conducted by Oesterle et al.[8,9]; 2) the tests conducted by Dazio et al.[11] on rectangular walls; 3) the tests on walls with highly confined boundary elements conducted by Hines et al.[12,13]; and 4) the aforementioned tests on U-shaped walls conducted by Beyer et al.[7] The cross sections, aspect ratios, and axial load ratios of these walls are given in Table 1. For the walls tested by Dazio et al.[11] and Beyer et al.,[7] the experimental measurements were available in electronic format and the shear deformations were evaluated according to the method developed by Hiraishi[10] (Eq. (2)). For the tests conducted

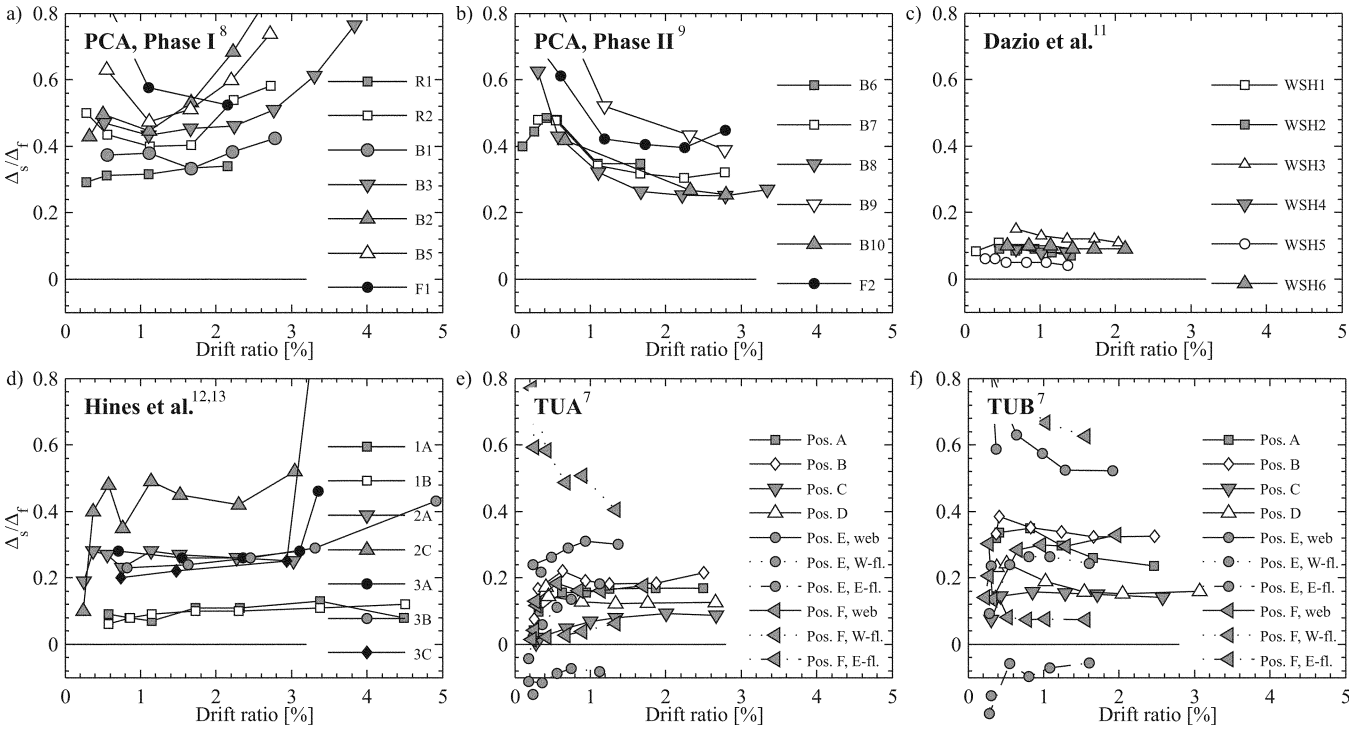

Fig. 6—Variation of Δ_s/Δ_f ratios with top drift for cantilever RC walls tested under quasi-static cyclic loading.

by Oesterle et al.[8,9] and Hines et al.,[12,13] the data were only available in the form of plots presented in the test reports, where the shear deformations had been evaluated according to Eq. (1(b)); this, of course, impairs the quality of the available results. The shear displacements reported in these test reports, however, are considered of sufficient accuracy for the following discussion.

Unlike Vallenas et al.,[20] Dazio[11] found that the ratio of shear-to-flexural displacements of the six capacity-designed RC walls with rectangular sections that were tested under quasi-static cyclic loading[11] remained approximately constant for the peak displacements of all cycles in the inelastic range; this is shown in Fig. 6(c). The ratios of shear-to-flexural displacements for the six walls vary between approximately 0.05 and 0.13. The walls tested by Dazio et al.[11] were all capacity-designed; therefore, their behavior was always controlled by flexure. To illustrate the difference for walls with shear-controlled behavior, the walls of Phase I of the PCA test series are discussed in the following. In this test series, Oesterle et al.[8] tested seven walls with different cross sections under unidirectional cyclic loading. No axial load was applied during these tests. Figure 6(a) shows the ratio of shear-to-flexural displacements as a function of the top drift. The Δ_s/Δ_f ratios in Fig. 6(a) are plotted for inelastic cycles only—small amplitude cycles at the beginning of the test and cycles at the end of the test when either bar fracture or web crushing had occurred and the capacity of the wall had significantly decreased are omitted. In the following, the variation of the Δ_s/Δ_f ratios for top displacements corresponding to a drift ratio of $\delta_{top} \geq 1\%$ is discussed. For these walls, a drift ratio of $\delta_{top} \geq 1\%$ corresponds to a displacement ductility between $\mu_\Delta = 1.6$ and 3.6, according to the yield displacements determined by Oesterle et al.[8]; hence, for $\delta_{top} \geq 1\%$, all walls are undergoing inelastic deformations. Figure 6(a) shows that for Walls R1 and B1, the Δ_s/Δ_f ratio is approximately constant over the entire ductility range. For the other four walls (Walls R2, B2, B3, and B5; Wall F1 is excluded because only two data points were available), the Δ_s/Δ_f ratio tended to increase with displacement demand for $\delta_{top} \geq 1\%$—that is, with increasing top displacement, the shear deformations contributed an increasing proportion of the total displacement. Differences between the two groups of specimens exist not only regarding the variation of the Δ_s/Δ_f ratio with ductility demand, but can also be found in their failure mechanisms: The first group—Specimens R1 and B1—failed in flexure and the shear transfer mechanism as such did not significantly deteriorate in both specimens. In the second group, the picture is less homogenous; but in all specimens, the shear-transfer mechanism significantly degraded before failure occurred. Specimens B2, B3, and B5 experienced abrasive rubbing of concrete and spalling of the concrete along inclined cracks through the web, which was most likely assisted by the absence of an axial force in the wall. As a result, the cracks were not properly closed upon load reversal and facilitated a deterioration of the crack interfaces. From the onset of the deterioration of the web concrete, the contribution of the shear deformations to the overall deformations significantly increased. Specimens B2 and B5 finally failed due to web crushing, whereas Specimen B3 failed due to fracture of the longitudinal reinforcing bars. Shortly before the bar fracture, however, the boundary element had sheared through. Specimen R2 was subjected to concrete crushing and also experienced large out-of-plane deformations due to instabilities of the wall under cyclic loading, which might have contributed to the deterioration of the compression struts and other parts of the shear-transfer mechanism.

Unlike the walls in the first phase, the walls that were tested in the second phase of the PCA tests were subjected to a constant axial load and all walls failed due to the sudden crushing of the compression struts.[9] The variation of Δ_s/Δ_f ratios with drift demand for these walls is shown in Fig. 6(b). Up to failure, the shear-transfer mechanism was not significantly degrading, and the ratio of shear-to-flexural displacements remained relatively constant (note that the cycles in which

the compression strut failure occurred are not included in Fig. 6(b) because for these cycles, the displacement components were not evaluated in the test report[9]). The same failure mechanism was observed for Test Units 3A, 3B, and 3C by Hines et al.[12,13] (Fig. 6(d)). The remaining test units in the study conducted by Hines et al.[12,13]—except for Unit 2B—failed due to buckling and fracture of the flexural reinforcement. The behavior of these test units was therefore flexure-controlled, and the Δ_s/Δ_f ratios of these walls were also approximately independent from the displacement demand. Test Unit 2B failed due to yielding of the shear reinforcement. As a result, the Δ_s/Δ_f ratios were very large (varying between 1.15 and 2.3 for drifts larger than 1%), and the corresponding results could not be plotted in Fig. 6(d). The behavior of the two U-shaped walls TUA and TUB (Fig. 6(e) and 6(f)) was also flexure-controlled and again the Δ_s/Δ_f ratios did not increase with ductility demand. Due to the bidirectional loading of these walls, however, the demand on the web and flanges varied considerably and led to a large variation of Δ_s/Δ_f ratios for the different loading directions; this will be discussed in more detail in the following section.

Although the shear-to-flexural displacement ratios vary considerably between the walls, for all the walls whose shear capacity did not significantly degrade, the shear-to-flexural displacement ratios remained approximately constant. For walls in which the shear-transfer mechanism was significantly degrading, the Δ_s/Δ_f ratio increases as the top displacement increases. One comes to the same conclusion if the stress state due to axial load, shear force, and moment of a cracked RC panel with parallel compression struts is considered. Figure 7(b) shows the Mohr's circle, representing the average strain state of the wall panel in Fig. 7(a). The variable ε_d refers to the axial strain in the compression strut (hence, $\varepsilon_d < 0$), ε_m refers to the mean axial strain, ε_h refers to the horizontal strain, γ refers to the shear strain, and β refers to the cracking angle measured against the element axis. Using the geometric relationships within Mohr's circle, the shear strain γ can be expressed as follows.

$$\gamma = \frac{\varepsilon_m}{\tan\beta} + \varepsilon_h \tan\beta - \frac{2\varepsilon_d}{\sin 2\beta} \quad (4)$$

The same equation is quoted in Oesterle et al.,[21] but it originates from Rabbat and Collins,[28] where it was given in a slightly different form. Although Eq. (4) only applies—strictly speaking—to a section of the wall that is small enough that the strain state is approximately homogenous, it can be used for visualizing the three different contributions to the shear strain γ. The first term represents the contribution of the mean axial strain ε_m. In structural walls subjected to seismic loading, the axial strains are chiefly caused by flexural deformations. Given that the depth c of the compression zone remains approximately constant once the section has yielded, ε_m is directly related to the curvature ϕ, which determines the flexural deformations. Therefore, the first term of Eq. (4) shows that the shear strains are directly related to the flexural strains. Hence, if the second and third terms are small, the shear displacements are proportional to the flexural displacements—this was, for example, the case for Dazio et al.'s[11] capacity-designed walls. The second term represents the contribution of the horizontal strains in the shear reinforcement to the shear strain and the third term represents the contribution of the strain in the compression

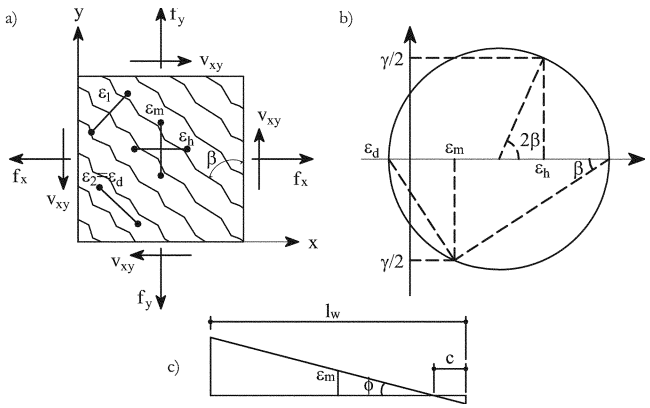

Fig. 7—(a) Truss analogy model for RC element with parallel compression struts; (b) Mohr's circle, representing strain state at center line of wall; and (c) strain profile showing ε_m and ϕ. Plots (a) and (b) are taken from Rabbat and Collins.[28]

diagonal to the shear strain. Thus, if the behavior of the wall is controlled by shear, and if plastic strains are accumulating in the shear reinforcement or the compression struts are softening considerably, the shear strains disproportionately increase to the flexural strains. Consequently, the Δ_s/Δ_f ratio increases with the top displacement demand. This was observed for some of the PCA test units of Phase I and Test Unit 2B tested by Hines et al.[12,13]

Variation of Δ_s/Δ_f ratio for U-shaped walls under bidirectional loading

The previous section showed that for walls controlled by flexure under unidirectional cyclic loading, the ratio of shear-to-flexural displacements remains approximately independent of the top displacement demand. This also holds approximately true for nonrectangular walls controlled by flexure if a specific loading direction is considered (Fig. 6(e) and 6(f)). For different directions of loading, however, the Δ_s/Δ_f ratios can vary significantly. This was shown by Thomson and Wallace[14] for a T-shaped wall loaded along its symmetry axis and it is illustrated herein by means of the U-shaped wall TUA tested under bidirectional loading.[7] Figure 8(a) shows the Δ_s/Δ_f ratios of the web and flanges for the five different directions of loading that were applied (Fig. 1). These ratios were computed as the average ratios of the approximately constant branches between $\delta \approx 0.6\%$ and the ultimate drift (Fig. 6(e)). Figure 8(b) shows the forces in the flanges and the web at peak displacements for the different directions of loading. Note that the rotation of the wall head about the vertical axis was restrained throughout the loading history (exceptions are outlined in Beyer et al.[7]); as a result, the flange forces are non-zero when the wall is loaded parallel to the web and unequally distributed when the wall is loaded in the diagonal direction.

Although the shear forces carried by the different wall sections (web and flanges) certainly influence the Δ_s/Δ_f ratios, they are not the only parameter. Figure 8(a) also shows that the Δ_s/Δ_f ratios tend to be larger if the wall section is under net axial tension. This applies, for example, to the web section ($\Delta_s/\Delta_f = 0.30$) when the wall is loaded to Position E or to the flange opposite the corner that is in compression ($\Delta_s/\Delta_f = 0.53$) when the wall is loaded to Position F. Out of the Δ_s/Δ_f ratios shown in Fig. 8(a), the negative ratio of the East flange ($\Delta_s/\Delta_f = -0.09$) at Position E

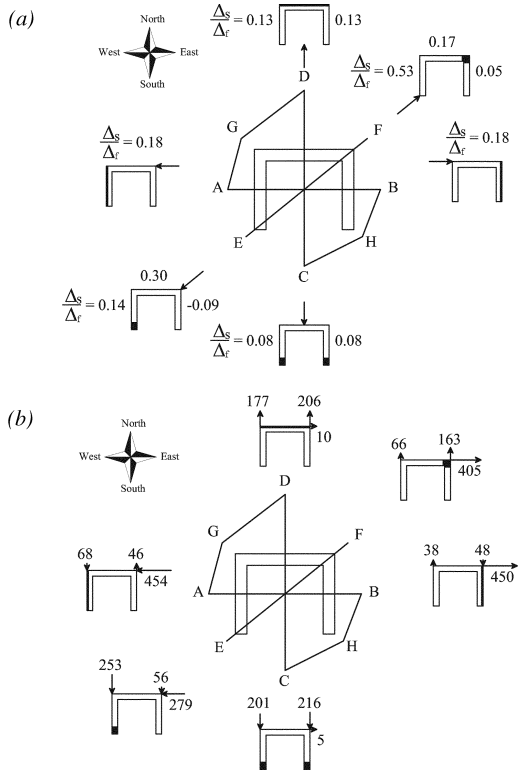

Fig. 8—For U-shaped wall TUA[7]: (a) average Δ_s/Δ_f ratios; and (b) actuator forces loading web and flanges at $\mu_\Delta = 4.0$. (Note: actuator forces are in kN; 1 kip = 4.448 kN.)

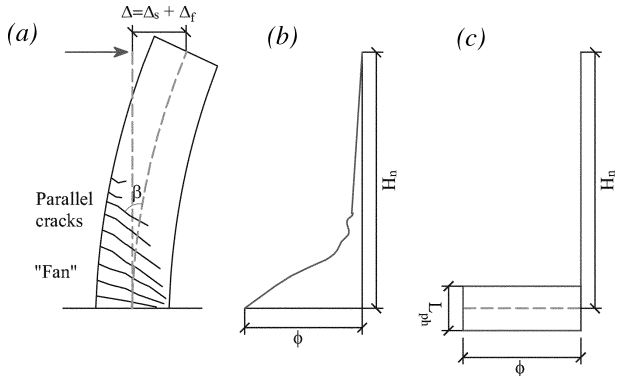

Fig. 9—Plastic hinge method: (a) crack pattern; (b) true curvature profile; and (c) plastic curvature profile assumed in plastic hinge method.

is most peculiar. When loading in the diagonal direction to Position E, the force in the East flange did not reach its peak at the maximum displacement but dropped from the force at zero displacement—which was required to restrain the rotation of the wall head—to the final value at Position E. This drop in force probably led to a reversal of the shear displacements in the East flange. Note that the same observation was made for the second U-shaped wall (TUB) tested by Beyer et al.[7] and also for the U-shaped walls tested by Pégon et al.[15-18]

EMPIRICAL MODEL FOR ESTIMATING RATIO OF SHEAR-TO-FLEXURAL DEFORMATIONS FOR WALLS CONTROLLED BY FLEXURE

To the authors' knowledge, there are only two equations at present for estimating the ratio of shear-to-flexural displacements, which are based on the observation that the ratio of shear-to-flexural displacement is approximately independent of the imposed ductility demand. The first is by Hines et al.[29] and the second is by Priestley et al.,[30] which is based on the work by Miranda et al.[31] Neither of the two accounts for the effect of the mean axial strain on the shear deformations. To complement their work, a new empirical equation is proposed for walls whose behavior is dominated by flexure. It is based on the assumption that the ratio of shear-to-flexural deformations in a wall whose shear-transfer mechanism is not significantly degrading depends on the geometry of the wall, the axial strain level within the wall, and the cracking angle. The proposed model is based on Eq. (4) in conjunction with the plastic hinge model (Fig. 9(c)). Over the height of the plastic hinge length L_{ph}, the curvature and the mean axial strain ε_m are assumed as constant. Therefore, for a given cracking angle, the shear strain γ over L_{ph} is also approximately constant (Eq. (4)). If it is further assumed that the contributions of the second and third term of Eq. (4) can be neglected and that the shear deformations outside the plastic hinge length are negligible, then the shear deformations can be estimated as

$$\Delta_s \approx \gamma L_{ph} \approx \frac{\varepsilon_m}{\tan\bar{\beta}} L_{ph} \tag{5}$$

where $\bar{\beta}$ is a cracking angle representative of the fanned crack pattern (Fig. 9(a)). The flexural deformations, on the other hand, are computed assuming that all inelastic flexural deformations can be ascribed to the plastic hinge mechanism.

$$\Delta_f \approx \theta \cdot H_n \approx \phi \cdot L_{ph} \cdot H_n \tag{6}$$

The ratio of shear-to-flexural deformations can therefore be written as

$$\frac{\Delta_s}{\Delta_f} \approx \frac{\varepsilon_m}{\phi \cdot \tan\bar{\beta}} \frac{1}{H_n} \tag{7}$$

where the quantities ε_m and ϕ are the axial strain at the center of the wall sections and the curvature, respectively, and are derived from the moment-curvature analysis. In this study, ε_m and ϕ were evaluated for the walls described in Table 1 for a maximum steel strain of 1.5%. The ratio ε_m-ϕ, however, remains typically quite stable along the inelastic branch of the moment-curvature relationship. For the U-shaped walls, moment-curvature analyses were carried out in the five different directions of loading that were applied during testing. For each direction of loading, the ε_m-ϕ ratios corresponding to the three wall sections of the U-shaped wall (web and two flanges) were determined by extracting the axial strain at the center of the wall section and dividing it by the curvature component associated with the in-plane bending moment of this wall. For a given ratio ε_m-ϕ (that is, for a given ratio of the compression zone c to the wall length l_w; refer to Fig. 7(c)), Eq. (7) yields that Δ_s/Δ_f is proportional to l_w/H_n. Equation (7) is therefore mainly a geometric relationship. It also accounts, however, for the fact that for the same wall subjected to different loading conditions, the ε_m-ϕ ratio might be different, as it was observed for U-shaped walls under bidirectional loading.

Because Eq. (7) is the result of a very simple concept regarding the shear deformations in conjunction with the plastic hinge model, it cannot capture the exact real behavior but only the main parameters that influence Δ_s/Δ_f. In particular, the following approximations are expected to affect the accuracy of Eq. (7):

- The plastic hinge length is calibrated to provide the best estimate of the top displacement Δ_f for a given curvature ϕ. The area underneath the curvature profile associated with the plastic hinge mechanism (Fig. 9(c)) is typically smaller than the area underneath the true curvature profile (Fig. 9(b)). Based on the observation that curvature and axial strain are directly proportional, the shear deformations are proportional to the area underneath the curvature profile. Hence, by approximating the structure with the plastic hinge mechanism in Fig. 9(c), the shear deformations are underestimated.
- Neglecting the second and third terms of Eq. (4), which represent the shear deformations due to strain in the horizontal reinforcement and strain in the compression strut, also underestimates the shear deformations.
- On the other hand, Eq. (7) will overestimate the Δ_s/Δ_f ratios because Eq. (6) is likely to underestimate the flexural deformations for a given curvature ϕ due to the fact that the elastic flexural displacement is also estimated on the basis of the plastic hinge model. Because L_{ph} is smaller than $H_n/3$ for slender walls, the curvature profile associated with elastic deformations leads to a larger top displacement Δ_f for the same base curvature than the plastic hinge mechanism.
- Equation (7) is written as a function of a cracking angle $\overline{\beta}$, which is representative of the plastic zone where the crack pattern is like a fan and the cracking angles vary between 90 degrees and β (Fig. 9(a)). It is desirable to express Eq. (7) as a function of the cracking angle β, which is the cracking angle outside the fan where cracks are approximately parallel. Hence, a correction factor should also account for the fact that the quotient $1/\tan\overline{\beta}$ is smaller than $1/\tan\beta$.

These approximations increase the scatter of the predicted-to-experimental Δ_s/Δ_f ratios but also bias the predicted Δ_s/Δ_f ratios. From the analysis of the walls considered in this study, it was found that a good estimate of a correction factor C_1 is 1.5. With $C_1 = 1.5$, Eq. (7) can be written as a function of $1/\tan\beta$ as

$$\frac{\Delta_s}{\Delta_f} = 1.5\frac{\varepsilon_m}{\phi}\tan\beta\frac{1}{H_n} \tag{8}$$

Equation (8) is applied to a database of walls that includes the walls tested by Oesterle et al.,[8,9] Dazio et al.,[11] Hines et al.,[12,13] and Beyer et al.,[7] which were already discussed in previous sections of this paper. Only those walls are included for which the experimentally determined Δ_s/Δ_f ratios were found to be approximately constant for top displacements corresponding to displacement ductilities larger than approximately 2. In addition, the U-shaped walls tested by Pégon et al.[15-18] and the tests on rectangular and T-shaped walls by Thomson and Wallace[14] are considered (Table 1). The data for the U-shaped wall tests by Pégon et al.[15-18] were available in electronic format and the shear deformations were evaluated according to the method developed by Hiraishi[10] (Eq. (2)). For the tests conducted by Thomson and Wallace,[14] the flexural deformations were computed as $\Delta_f = \Delta - \Delta_s$ because the variation of curvature over the height of the wall was not measured. The shear deformations were computed by Thomson and Wallace[14] according to the method developed by Hiraishi,[10] assuming a value of 2/3 for α.

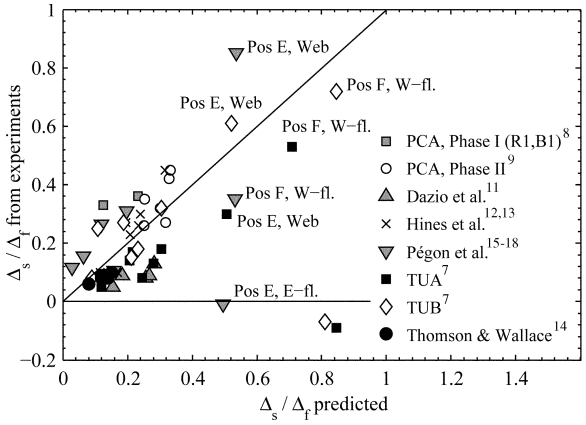

Fig. 10—Comparison of predicted Δ_s/Δ_f ratios to ones determined from experimental measurements.

Figure 10 shows the comparison of the Δ_s/Δ_f ratios predicted with Eq. (8) and the experimentally determined ratios. These predictions were obtained using the cracking angles observed during the experiments. For design purposes, the cracking angle needs to be estimated. As an approximate estimate, a cracking angle of 45 degrees can be assumed. A better estimate is obtained with the following equation by Collins and Mitchell[32]

$$\beta = \tan^{-1}\left(\frac{jd}{V}\left(f_1 b_w + \frac{A_{sw} f_{yw}}{s}\right)\right) < 90° \tag{9}$$

where jd is the lever arm between the compression and tensile resultant; V is the shear force; f_1 is the tensile strength orthogonal to the crack, which can be estimated as a function of the cracking stress and the strain orthogonal to the crack[32]; b_w is the wall thickness; and A_{sw}, f_{yw}, and s are the area, yield strength, and spacing of the shear reinforcement, respectively. For most of the considered walls, the agreement between the predicted and experimentally determined Δ_s/Δ_f ratios in Fig. 10 is satisfactory. The exceptions are the negative ratios of the U-shaped walls, which cannot be captured (refer to the previous section). It is emphasized that the variety of methods for measuring and evaluating the shear deformations causes an inter-test series variability of the Δ_s/Δ_f ratios, which adds to the generally known scatter of shear-related quantities. The error can be assessed by comparing the sum of the displacement components to the total measured displacements. For example, for Test Units R1 and B1 of Phase I of the PCA tests, the sum of the shear and flexural displacements is approximately 15% larger than the measured total displacement. Part of the discrepancy can be attributed to evaluating the shear displacements according to Eq. (1(b)), which overestimates the shear displacements, rather than using Eq. (2). As an alternative, the shear deformations could be evaluated as the difference between the total and flexural deformations—that is, $\Delta_s = \Delta - \Delta_f$. With this approach, the average Δ_s/Δ_f ratios of Test Units R1 and B1 would decrease from 0.33 and 0.36 to 0.15 and 0.21, respectively, which would agree significantly better with the

predicted Δ_s/Δ_f ratios. This example illustrates the large sensitivity of the Δ_s/Δ_f ratios to the selected evaluation method. Despite these uncertainties, Fig. 10 shows that Eq. (8) is able to capture the general trend in the variation of the Δ_s/Δ_f ratios.

SUMMARY AND CONCLUSIONS

At present, when slender RC structural walls controlled by flexure are modeled by means of beam elements and analyzed for their seismic behavior in the inelastic range, it is often assumed that the shear stiffness remains constant throughout the loading process and that the shear deformations—once the nominal strength is reached—do not increase. The purpose of this paper was to show by means of experimental results from quasi-static tests on RC structural walls that these assumptions do not hold true. Many of the observations are not new but have already been made as early as the 1970s by Wang et al.,[26] Vallenas et al.,[20] and Oesterle et al.,[8,9,21] who all observed that for increasing top displacements, the ratio of shear-to-flexural displacements remained either approximately constant or even grew with increasing displacement demand. Based on their findings and the evaluation of other quasi-static cyclic tests, the following observations were made:

- For RC walls forming a flexural hinge and a stable shear-transfer mechanism, the ratio of shear-to-flexural displacement remains approximately constant over the entire ductility range once the walls have reached their nominal strength. A stable shear-transfer mechanism requires that the shear reinforcement remain largely elastic, the concrete diagonal does not crush, and other mechanisms—such as the abrasive rubbing of concrete along inclined cracks—are limited. For these walls, the shear stiffness at peak displacements decreases in a similar proportion as the flexural stiffness of the structural wall. This behavior was observed for walls whose behavior was controlled by flexure. It seems also applicable for the cycles before the onset of crushing to walls that failed due to sudden crushing of the concrete diagonal.
- If the shear-transfer mechanism is significantly degrading, the shear deformations increase in larger proportion than the flexural deformations. For these walls, the ratio of shear-to-flexural displacements tends to increase with ductility demand. In these cases, the Δ_s/Δ_f ratios are also strongly dependent on the loading history. This behavior was observed for walls whose behavior was controlled by shear.
- The shear strain distribution over a wall is not even. Demec measurements showed that shear strains concentrate in regions where the axial strains are large—that is, in regions where the wall undergoes inelastic deformations. This was also confirmed by the experimental results of U-shaped walls, which showed that the Δ_s/Δ_f ratios were particularly large for those wall sections and loading directions that led to large tensile strains in the considered wall section.
- For nearly half of the considered cantilever walls (the different loading directions and wall sections of the U-shaped walls were separately counted), the shear deformations constituted more than 20% of the flexural deformations when the walls responded in the inelastic range. Hence, the shear deformations of RC walls—even if they are controlled by flexure—should be considered when analyzing the seismic behavior of such walls. The contribution of the shear deformations to the total deformation is larger for shorter walls. Even in very slender walls, however, the shear flexibility of walls might need to be considered when assessing interstory drifts at the level where the flexural deformations concentrate. Due to shear deformations, the interstory drifts at this level will be appreciably larger than anticipated if only flexural deformations are considered. Therefore, deformation demands on other structural and nonstructural elements at this level will also be larger.
- The results were summarized in a simple model for estimating the Δ_s/Δ_f ratios for walls controlled by flexure. Such estimates allow the engineer to evaluate the expected shear deformations based on the flexural displacement or to compute approximate shear stiffnesses for a given top displacement level that can be used in conjunction with beam models. An example in which this method has been applied is given in Beyer et al.[33]

The analysis of the different walls has also shown that—unlike for flexural displacements—different evaluation techniques have been used for evaluating the experimental shear displacements. Some of these methods have been found erroneous[10] and should not be used when computing the shear displacement component from structural wall tests. This will also contribute to a more homogenous set of experimental data for shear deformations and help to reduce the inter-serial scatter between test series.

ACKNOWLEDGMENTS

The authors would like to thank P. Pégon from the Joint Research Centre (JRC) in Ispra, Italy, for sharing the test data and reports of the U-shaped wall tests that were carried out at the JRC. The authors would also like to thank J. W. Wallace from the University of California, Los Angeles, CA, for making the report on the tests he performed at Clarkson University available.

REFERENCES

1. Vecchio, F. J., and Collins, M. P., "The Modified Compression-Field Theory for Reinforced Concrete Elements Subjected to Shear," ACI JOURNAL, *Proceedings* V. 83, No. 2, Mar.-Apr. 1986, pp. 219-231.

2. Bentz, E., *Response-2000, Shell-2000, Triax-2000, Membrane-2000 User Manual*, University of Toronto, ON, Canada, 2001, 85 pp.

3. Wong, P. S., and Vecchio, F. J., *VecTor2 and Formworks User's Manual*, University of Toronto, ON, Canada, 2002, 213 pp.

4. CSI, "PERFORM 3Dv4—Nonlinear Analysis and Performance Assessment for 3D Structures," Computer and Structures, Inc., Berkeley, CA, 2006, 328 pp.

5. Bathe, K.-J., *Finite Element Procedures*, Prentice Hall, Upper Saddle River, NJ, 1996, 1037 pp.

6. Taucer, F. F.; Spacone, E.; and Filippou, F. C., "A Fiber Beam-Column Element for Seismic Response Analysis of Reinforced Concrete Structures," *Report* No. UCB/EERC-91-17, University of California, Berkeley, Berkeley, CA, 1991, 139 pp.

7. Beyer, K.; Dazio, A.; and Priestley, M. J. N., "Quasi-Static Cyclic Tests of Two U-Shaped Reinforced Concrete Walls," *Journal of Earthquake Engineering*, V. 12, No. 7, 2008, pp. 1023-1053.

8. Oesterle, R. G.; Fiorato, A. E.; Johal, L. S.; Carpenter, J. E.; Russell, H. G.; and Corley, W. G., "Earthquake Resistant Structural Walls—Tests of Isolated Walls," *Report to National Science Foundation*, PCA Construction Technology Laboratories, Skokie, IL, 1976, 317 pp.

9. Oesterle, R. G.; Aristizabal-Ochoa, J. D.; Fiorato, A. E.; Russell, H. G.; and Corley, W. G., "Earthquake Resistant Structural Walls—Tests of Isolated Walls—Phase II," *Report to National Science Foundation*, PCA Construction Technology Laboratories, Skokie, IL, 1979, 332 pp.

10. Hiraishi, H., "Evaluation of Shear and Flexural Deformations of Flexural Type Shear Walls," *Bulletin of the New Zealand Society for Earthquake Engineering*, V. 17, No. 2, 1984, pp. 135-144.

11. Dazio, A.; Wenk, T.; and Bachmann, H., "Versuche an Stahlbetontragwänden unter Zyklisch-Statischer Einwirkung (Quasi-Static Cyclic Tests on RC Structural Walls)," *Report* No. 239, ETH, Zurich, Switzerland, 1999, 160 pp.

12. Hines, E. M.; Seible, F.; and Priestley, M. J. N., "Cyclic Tests of Structural Walls with Highly-Confined Boundary Elements," *Report* No. SSRP-99/15, University of California, San Diego, San Diego, CA, Aug. 1999, 266 pp.

13. Hines, E. M.; Dazio, A.; and Seible, F., "Seismic Performance of Hollow Rectangular Reinforced Concrete Piers with Highly-Confined Boundary Elements Phase III: Web Crushing Tests," *Report* No. SSRP-2001/27, University of California, San Diego, San Diego, CA, June 2002, 239 pp.

14. Thomson IV, J. H., and Wallace, J. W., "Displacement-Based Design of RC Structural Walls: An Experimental Investigation of Walls with Rectangular and T-Shaped Cross Sections," *Report* No. CU/CEE-95/06, Clarkson University, New York, 1995, 373 pp.

15. Pégon, P.; Plumier, C.; Pinto, A.; Molina, J.; Gonzalez, P.; Colombo, A.; Tognoli, P.; Hubert, O.; and Tirelli, D., "U-Shaped Walls: Description of the Experimental Set-Up," TMR-ICONS-TOPIC5, JRC Special Publication No. I.00.141, JRC Ispra, Italy, 2000, 40 pp.

16. Pégon, P.; Plumier, C.; Pinto, A.; Molina, J.; Gonzalez, P.; Tognoli, P.; and Hubert, O., "U-Shaped Walls: Quasi-Static Test in the X and Y Directions—Test Report," TMR-ICONS-TOPIC5, JRC Ispra, Italy, 2000, 25 pp.

17. Pégon, P.; Plumier, C.; Pinto, A.; Molina, J.; Gonzalez, P.; Tognoli, P.; and Hubert, O., "U-Shaped Walls: Quasi-Static Test in the Y Direction—Test Report," TMR-ICONS-TOPIC5, JRC Ispra, Italy, 2000, 19 pp.

18. Pégon, P.; Plumier, C.; Pinto, A.; Molina, J.; Gonzalez, P.; Tognoli, P.; and Hubert, O., "U-Shaped Walls: Quasi-Static Test in the X Direction—Test Report," TMR-ICONS-TOPIC5, JRC Ispra, Italy, 2000, 25 pp.

19. Massone, L. M., and Wallace, J. W., "Load-Deformation Response of Slender Reinforced Concrete Walls," *ACI Structural Journal*, V. 101, No. 1, Jan.-Feb. 2004, pp. 103-113.

20. Vallenas, J. M.; Bertero, V. V.; and Popov, E. P., "Hysteretic Behaviour of Reinforced Concrete Structural Walls," *Report* No. UBC/EERC-79/20, University of California, Berkeley, Berkeley, CA, 1979, 234 pp.

21. Oesterle, R. G.; Aristizabal-Ochoa, J. D.; Shiu, K. N.; and Corley, W. G., "Web Crushing of Reinforced Concrete Structural Walls," ACI JOURNAL, *Proceedings* V. 81, No. 3, May-June 1984, pp. 231-241.

22. FEMA 356, "Prestandard and Commentary for the Seismic Rehabilitation of Buildings," Federal Emergency Management Agency, Washington, DC, 2000, 518 pp.

23. ACI Committee 318, "Building Code Requirements for Structural Concrete (ACI 318-08) and Commentary," American Concrete Institute, Farmington Hills, MI, 2008, 473 pp.

24. Timoshenko, S. P., *Theory of Elasticity*, McGraw-Hill, New York, 1934.

25. Park, R., and Paulay, T., *Reinforced Concrete Structures*, John Wiley & Sons, Inc., New York, 1975, 800 pp.

26. Wang, T. Y.; Bertero, V. V.; and Popov, E. P., "Hysteretic Behaviour of Reinforced Concrete Framed Walls," *Report* No. UBC/EERC-75/23, University of California, Berkeley, Berkeley, CA, 1975, 367 pp.

27. Dazio, A., "Entwurf und Bemessung von Tragwandgebäuden unter Erdbebeneinwirkung (Seismic Design of Buildings with Structural Walls)," PhD thesis No. 13739, ETH, Zurich, Switzerland, 2000, 229 pp.

28. Rabbat, B. G., and Collins, M. P., "A Variable Angle Space Truss Model for Structural Concrete Members Subjected to Complex Loading," *Proceedings of the Douglas McHenry International Symposium on Concrete and Concrete Structures*, SP-55, American Concrete Institute, Farmington Hills, MI, 1978, pp. 547-587.

29. Hines, E. M.; Restrepo, J. I.; and Seible, F., "Force-Displacement Characterization of Well-Confined Bridge Piers," *ACI Structural Journal*, V. 101, No. 4, July-Aug. 2004, pp. 537-548.

30. Priestley, M. J. N.; Calvi, G. M.; and Kowalsky, M. J., *Displacement-Based Seismic Design of Structures*, IUSS Press, Pavia, Italy, 2007, 721 pp.

31. Miranda, P. A.; Calvi, G. M.; Pinho, R.; and Priestley, M. J. N., "Displacement-Based Assessment of RC Columns with Limited Shear Resistance," *Report ROSE-2005/04*, IUSS Press, Pavia, Italy, 176 pp.

32. Collins, M. P., and Mitchell, D., *Prestressed Concrete Structures*, Response Publications, Toronto, ON, Canada, 1997, 766 pp.

33. Beyer, K.; Dazio, A.; and Priestley, M. J. N., "Inelastic Wide-Column Models for U-Shaped Reinforced Concrete Walls," *Journal of Earthquake Engineering*, V. 12, No. SP1, 2008, pp. 1-33.